Stellar oscillations induced by the passage of a fast stellar object

Author: Michael Naizer
Advisor: Carlos Bertulani, **Collaborator:** William Newton

April 8, 2014

Abstract

We investigate induced oscillations by the gravitational field of a fast stellar object, such as a neutron star or a black-hole in a near miss collision with another star. The non-adiabatic collision condition leads to possible large amplitude oscillations in the star. We show that for a solar-type star a resonant condition can be achieved by a fast moving stellar object with velocity in the range of 100 km/s to 1000 km/s, passing at a distance of a few multiples of the star radius. Although such collisions are rare, they are more frequent than head-on collisions, and their effects could be observed through a visible change of the star luminosity within a few hours.

In addition, we have studied a set of equations of state for the description of neutron stars. This will be useful for an extension of the present work to stellar collision models which include the dependence of the stellar oscillations on the compressibility of compact stars.

Contents

1 Introduction and Motivation

1.1 Existing Stellar Oscillation Models

There have been a number of attempts to model stellar oscillations in astrophysics [1] [2] [3]. Most of these methods are descriptive rather than predictive, and attempts to predict stellar oscillations caused by an interaction between two or more stars have been relatively unexplored. What research has been done in predicting oscillations is mostly dealing with the interactions between two stars in a binary system or the process of binary formation [4] [5] [6]. In this study, we predict stellar oscillations induced during a close collision between stars, or between a black-hole and a star. This phenomenon has not been much explored in existing literature.

There are a variety of very precise models to describe stellar oscillations which include a full hydrodynamical treatment of a star's matter. By using such models one can for example track small oscillations in the Sun, where they can be observed to a very high precision (over 1000 separate oscillation modes have been observed [7]). However, if a close collision with a fast stellar object were to occur with our Sun, it would almost certainly emit enough radiation or alter the Earth's to destroy life on the planet. We are here for a long time, thus such close encounters are rare and our concern is really with the probabilistic distribution of such events in the galaxy and beyond it. The high degree of accuracy obtained with elaborated hydrodynamical models is not necessary since we have been so far unable to observe such collision-driven oscillations, and any observation would be restricted at best to very dramatic phenomena with the emission of large amounts of radiation. For this reason, and for computational simplicity, we consider a simple model for "bulk stellar oscillations" based on a incompressible fluid, rather than borrowing one of the previousy developed hydrodynamical models.

1.2 Kepler Orbits

There are three types of Kepler orbits which describe the trajectories of two gravitationally interacting massive objects. These three trajectories are differentiated by a parameter called *eccentricity*, e, which describes how "curved" the path is:

1. Elliptical Orbit ($e < 1$)
2. Parabolic Trajectory ($e = 1$)
3. Hyperbolic Trajectory ($e > 1$).

As the names suggest, the elliptical orbit follows the shape of an ellipse, the parabolic trajectory a parabola, etc. A circular orbit is the most "curved" orbit possible, and is a special type of elliptical orbit where $e = 0$. As e takes on higher values, the trajectory becomes less curved, eventually looking like a straight line. This is important, first of all, because while the first forms a closed loop, the latter two are called "open" or "unbound" and objects involved in such trajectories will continue moving out to an infinite distance. As mentioned earlier, the prediction of stellar oscillation has up until now been almost exclusively confined to the first two (more about this in Section 2.6).

1.3 Stars

Since we are interested in a largely unexplored phenomenon, we will use a much simplified stellar model. In our model, stars are assumed to be homogenous and composed of incompressible matter. Although this is not the most physically accurate stellar model, it will vastly reduce the complexity of the problem and give a reasonable estimate for the bulk properties of stars involved in the collision. Our adopted model is developed in the most general way so that it can be applied to any stellar object, including compact stars such as white dwarfs and neutron stars. Although in the case of a nearby collision of neutron stars, the gravitation may be so high that relativity would be required to solve the problem accurately. We do not consider such relativistic corrections, implying that our results for neutron stars collisions may be significantly less accurate than results for other types of star. The scope of this project covers the following different types of stars, each of which has a unique size, mass, and composition:

1.3.1 Main Sequence (MS) Star

Main sequence stars make up the majority of stars in the universe. MS stars vary widely in size and mass (masses $\approx 0.1 - 40M_\odot$, radii $\approx 0.1 - 18R_\odot$). For the most part, MS stars follow the laws of an ideal gas, and have an equation of state based on the ideal gas law. However, some MS stars in the high and low size ends have a slightly different structure and equation of state than their average counterparts. For instance, extremely large stars are supported strongly by radiation pressure, and solar-type stars are more supported by gas pressure. Consequently, there is much variation in the masses and radii of MS stars.

1.3.2 White Dwarf (WD)

Much smaller and more dense than a MS star (mass $\approx 0.6 - 1.4M_\odot$, radius $\approx 0.01R_\odot$), a white dwarf is the eventual end product when an average-sized MS star exhausts all its hydrogen and helium fuel. In all but the most massive stars, at this point nuclear reactions cease to occur, so the star cools and contracts. Unlike MS stars, which are supported against gravity by gas pressure, white dwarfs are supported by degenerate particle pressure from quantum mechanics. In short, the Pauli exclusion principle states that no two electrons may occupy the same space. As gravity compresses the particles in the star, the electrons are forced closer and closer together, but their resistance against occuping the same state opposes the attractive force of gravity. This results in a star with very different properties and a different density distribution than the main sequence.

1.3.3 Neutron Star (NS)

Even more dense than a white dwarf (mass $\approx 1.4 - 3M_\odot$, radius $\approx$ 12km), a neutron star is the eventual end product in the lifecycle of a very large star. Similar to WD, NS are supported against gravity by the degenerate pressure of nuclear matter, and follow a unique equation of state. The matter in neutron stars is so dense that the non-relativistic equation of hydrostatic support is no longer valid. Instead, a specialized equation called the Tolman-Oppenheimer-Volkoff (TOV) equation has been derived from Einstein's field equations to produce a solution with relativistic corrections which is applicable to a NS.

Our initial intention was to focus on modeling neutron star oscillations. However, preliminary results showed us that the effect on NS would be small, due to the high stiffness (incompressibility) of such stars. With this realization, we shifted the focus onto sun-like main sequence stars, which are far less dense and therefore respond more to the interactions of interest. I should note that conditions inside a NS are so exotic that nothing like NS matter can be duplicated on Earth, so much of the internal dynamics of these objects remains a mystery. As such, NS are really the most interesting of the stars considered here, although their limited response to oscillation slightly shadows this fact. My interest in neutron stars began long before this project was initialized, when I worked with Dr. Bertulani and Dr. Newton on modeling the large-scale properties of NS based on the equation of state. Since the equation of state determines certain large-scale properties (mass and radius) of NS, and also has an impact on the oscillations studied here, a summary of my previous work on equations of state for neutron stars has been included in Section 4.

1.3.4 Black Hole (BH)

Although not technically a star, a black hole is a massive astronomical object which is suspected to be a remnant from the core collapse of an extremely massive star, with $m_s \gtrsim 8M_\odot$. In general, BH are defined by their famous property that the escape velocity of any particle (including light) has to be greater than the speed of light. That is, a BH is so massive that even light cannot escape its gravity. According to the *No-Hair Theorem*, the only observable properties of BH are mass, electric charge, and rotation. Black hole oscillations (if they occur) are therefore impossible to observe, so a black hole can only serve as the passing massive object in our model, where it is characterized only as a point mass with some translational velocity.

1.4 Hypervelocity Stars

Several stars in our galaxy have been observed with velocities of 1000 km/s or faster [8]. This is to be compared with the average stellar velocity, which is on the order of 100 km/s. When one of these hypervelocity

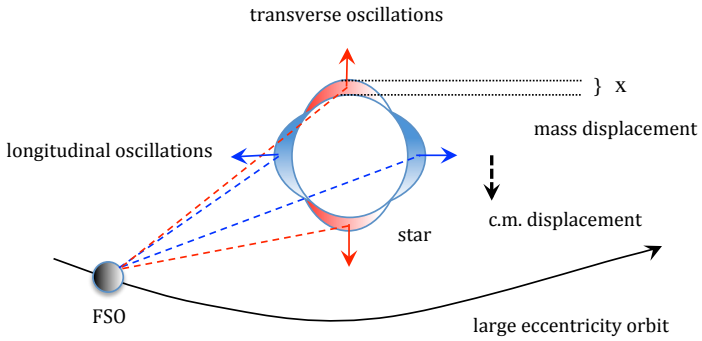

Figure 1: Schematic view of the effect of gravitation on a mass element of a star due to the passage of a fast stellar object.

stars passes nearby another main sequence star, interesting things can happen. Because in this case (see estimates below) the natural harmonic oscillation frequency of the star is around the same value as the inverse of the collision time of a hypervelocity star, the oscillations due to this interaction will be closer in resonance with the gravitational interaction than in a collision with a smaller stellar velocity.

2 Forced Oscillations by a Time-Dependent Gravitational Force

2.1 Tidal Force

To begin with, we consider Newton's equation for universal gravitation between two bodies

$$\mathbf{F}(\mathbf{r}) = -\frac{GMdm_s}{|\mathbf{r}|^2}\hat{\mathbf{r}}, \tag{1}$$

where G is the gravitational constant, M is the mass of the fast stellar object (FSO), dm_s is the mass the volume element within the star, and $\mathbf{r}$ is the vector coordinate between M and dm_s.

The gravitational potential is the potential energy per unit mass at a certain location in the system, i.e.,

$$V(\mathbf{r}) = -\frac{GM}{|\mathbf{r}|}. \tag{2}$$

As shown in figure 1, we define the vector $\mathbf{R}(t)$ as the distance between the center of mass of the FSO and the star, and $\mathbf{x}$ to be the distance from the center of the star to the mass element dm_s of the star. This allows us to express the gravitational potential at position $\mathbf{x}$ inside the star as

$$V(\mathbf{x},t) = -\frac{GM}{|\mathbf{R}(t)-\mathbf{x}|}. = -\frac{GM}{\sqrt{R^2(t)-2\mathbf{x}\cdot\mathbf{R}(t)+x^2}}. \tag{3}$$

Since $R > x$ at all times (the FSO does not pass inside in the star), this equation can be expanded into a series of Legrende polynomials of degree l,

$$V(\mathbf{x},t) = -GM\sum_{l=0}^{\infty}\frac{x^l}{R^{l+1}(t)}P_l(\cos\gamma). \tag{4}$$

According to the addition theorem of spherical harmonics,

$$P_l(\cos\gamma) = \frac{4\pi}{2l+1}\sum_{m=-l}^{l}Y_{lm}^*(\hat{\mathbf{R}})Y_{lm}(\hat{\mathbf{r}}), \tag{5}$$

where Y_{lm} are the spherical harmonic functions. Combining these two equations,

$$V(\mathbf{x},t) = -GM \sum_{m=-l}^{l} \frac{4\pi}{2l+1} Y_{lm}(\hat{\mathbf{R}}(t)) \frac{x^l}{R^{l+1}(t)} Y^*_{lm}(\hat{\mathbf{x}}). \tag{6}$$

This is a sum of terms with *multipole of degree* (or order) l, following the convention of spherical harmonics. The lower multipoles are named according to 2^l: monopole, dipole, quadrupole, octopole, etc. In general, the lower multipoles have a larger magnitude (due to the $1/R^l$ term). Hence, we will focus on the lowest multipole orders as we will consider small amplitude oscillations (in fact, only the quadrupole, $l = 2$). The zero-th order can be negelected because it will only induce the center of mass motion of the whole star. For cylindrically symmetric mass distributions, the $l = 1$ *dipole* term, will also disappear. Thus, the lowest order term is $l = 2$, *quadrupole* or *tidal* potential. Higher multipole degrees are possible, such as the octupole, but they are orders of magnitude smaller and therefore will be neglected in this study.

We give an idea on how the tidal force shows up from Eq. (6). It is easy to see from this equation that for the quadrupole order[1] only the squares of the intrinsic coordinates $\mathbf{x} \equiv (x, y, z)$ with show up,

$$V(x,t) \sim \frac{GMx^2}{R^3(t)}, \tag{7}$$

which leads to the potential energy dU of masses M and dm_s

$$dU(x,t) = V(x,t)dm_s \sim \frac{GMx^2 dm_s}{R^3(t)}, \tag{8}$$

from which we can calculate the force on the mass element dm_s, using the fact that $dF_x = \partial_x(dU)$:

$$dF(x,t) \sim \frac{GMx dm_s}{R^3(t)}. \tag{9}$$

The force per unit mass dm_s, will then be given by

$$f(x,t) \sim \frac{GMx}{R^3(t)}. \tag{10}$$

This is the origin of the *tidal* force, which tends to elongate the mass distribution towards the poles [9]. The same treatment can be used for all cartesian components.

A proper account for all factors appearing in Eq. (6) can be obtained by applying $F = -\nabla U$ directly to it after integration over the whole density of the star, i.e.,

$$F_{tot}(t) = -\nabla_\xi \int V(\mathbf{x},t)\rho(\mathbf{x},t)d^3x, \tag{11}$$

where $\mathbf{x}$ denotes the intrinsic coordinate of the mass element $dm_s \equiv \rho(\mathbf{x})d^3x$ and ξ denotes the average displacement of mass within the whole star. For an incompressible fluid, only the parts of the star near the poles with contribute to the *effective mass* for the oscillations (as shown in figure 2). In fact, ξ will measure the mass displacement from the star's spherical shape equilibrium. The exact value of this effective mass and displacement from equilibrium depends on the model one adopts for the star, including its hydrodynamical behavior. Eq. (10) will reduce to a force per effective mass. In the incompressible fluid model the effective mass $\mathcal{M}_l$ is given below. To alleviate the notation, we next will use x instead of ξ for its displacement from equilibrium.

2.2 Driven Oscillator Model

We consider the material within a star being pulled away from its equilibrium position to undergo harmonic oscillation like a mass attached to a spring. The relevant forces acting on this "spring" are:

[1] Here we only discuss one dimension for simplicity.

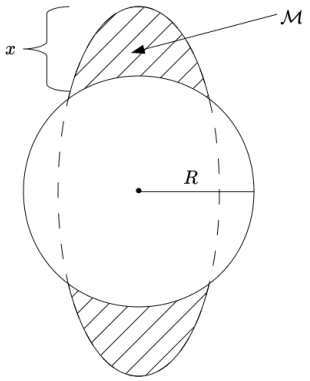

Figure 2: Schematic diagram illustrating the meaning of effective mass $\mathcal{M}$ and effective displacement x in the case of an exaggerated deformation.

- $\mathbf{F}_g$, the gravitational force exerted by the passing object pulling the mass apart from their equilibrium position - Eq. (9);
- $\mathbf{F}_s$, the combination of internal forces pulling the star's matter back into equilibrium;
- $\mathbf{F}_v$, the frictional force caused by the viscosity of stellar gas and radiation, which acts to slow down the oscillation.

During the collision event, these forces are unbalanced, which causes a net acceleration $\mathbf{a}$ on the matter in the star. According to Newton's 2nd Law:

$$\mathbf{F}_g - \mathbf{F}_s - \mathbf{F}_v = m\mathbf{a}, \tag{12}$$

where m is the amount of mass in the star involved in the oscillation (the effective mass, mentioned above).

According to Hooke's Law for a driven damped harmonic oscillator, the restorative force $\mathbf{F}_s$ is defined as being proportional to the displacement, or

$$\mathbf{F}_s(t) = -k\mathbf{x}(t), \tag{13}$$

where k is called the stiffness parameter, and is dependent on the internal properties of the star. The frictional force is given by

$$\mathbf{F}_v(t) = -\gamma\dot{\mathbf{x}}(t), \tag{14}$$

where γ is the frictional parameter and the notation $\dot{x} = \frac{\partial}{\partial t}(x)$.

Using the definitions of each of the forces in equation (12), we have

$$\mathbf{F}_g(t) = m\ddot{\mathbf{x}}(t) + \gamma\dot{\mathbf{x}}(t) + k\mathbf{x}(t), \tag{15}$$

where $\ddot{\mathbf{x}} = \partial^2\mathbf{x}/\partial t^2 = \mathbf{a}(t)$. Now, if we define the force per unit mass $\mathbf{f}(t) = \mathbf{F}_g(t)/m$, and the variables $\beta = \gamma/2m$ and $\omega_0 = \sqrt{k/m}$, then we get

$$\mathbf{f}(t) = \ddot{\mathbf{x}}(t) + 2\beta\dot{\mathbf{x}}(t) + \omega_0^2\mathbf{x}(t). \tag{16}$$

This equation describes a driven damped harmonic oscillator which will be the basis of our stellar oscillation model.

2.3 Inertial and Stiffness Parameters

In our simplified stellar model, a star is assumed to be composed of incompressible matter with a uniform density of $\rho = 3m_s/(4\pi r_s^3)$, where m_s is the mass and r_s is the radius of the star at equilibrium. This model, originally due to Lord Kelvin can be used to describe multipole oscillations in an incompressible homogenous sphere [10]. At multipole order l, the natural harmonic frequency is given by

$$\omega_0^2 = \frac{\mathcal{K}_l}{\mathcal{M}_l} = \frac{2l(l-1)}{2l+1}\frac{Gm_s}{r_s^3}, \tag{17}$$

where $\mathcal{M}_l$ is the inertial parameter (effective mass, see Section 2.1), and $\mathcal{K}_l$ is the stiffness parameter. For the quadrupole order $l = 2$, we get the following in terms of the star's average density ρ_0,

$$\omega_0^2 = \frac{4}{5}\frac{Gm_s}{r_s^3} = \frac{16\pi G\rho_0}{15}. \tag{18}$$

For small amplitude multipole oscillations the inertia parameter has been deduced in Ref. [11],

$$\mathcal{M}_l = \frac{3}{l(2l+1)} m_s r_s^2. \tag{19}$$

which implies an effective mass equal to

$$\mathcal{M}_2 = \frac{3m_s r_s^2}{10}. \tag{20}$$

The stiffness parameter becomes

$$\mathcal{K}_2 = \omega_0^2 \mathcal{M}_2 = \frac{6Gm_s^2}{25r_s}. \tag{21}$$

These values of the effective mass and stiffness parameter can now be used in equation (16) with $m \to \mathcal{M}_2$. The stiffness parameter is intrinsic to ω_0.

2.4 Friction Parameter

Inside the star, there are a number of sources of friction [12],

- Gas Viscosity: $\gamma_g \sim T^{5/2}$,
- Radiative (Jeans) Viscosity: $\gamma_r \sim T^4$,
- Turbulence: $\gamma_t = R_e\gamma_r/3$,

where T is the local temperature of the star and R_e is the Reynolds number, which is dependent on the mean free path and velocity of individual particles. The total friction parameter γ is the sum of all three contributions. For typical main sequence stars, the radiative portion dominates over the gas portion in the star's interior, but these two parts are more balanced in the outer layers. At high Reynolds numbers ($R_e \sim 10^3 - 10^4$), turbulence can occur which will then dominate all other forms of friction. In short, these equations require a much more precise stellar model which includes a radial temperature gradient and information on the motion of individual particles for the star. Instead, we adopt a simpler model of the form

$$\gamma = A_\gamma \mathcal{M}_2 \omega_0, \tag{22}$$

with A_γ taken as a free parameter. We are then free to choose value for A_γ which resembles approximately the conditions in a star. In the case of the results presented here, we use $A_\gamma = 0.1$ and the results do not change appreciably much in the range $A_\gamma = 0.1 - 0.5$.

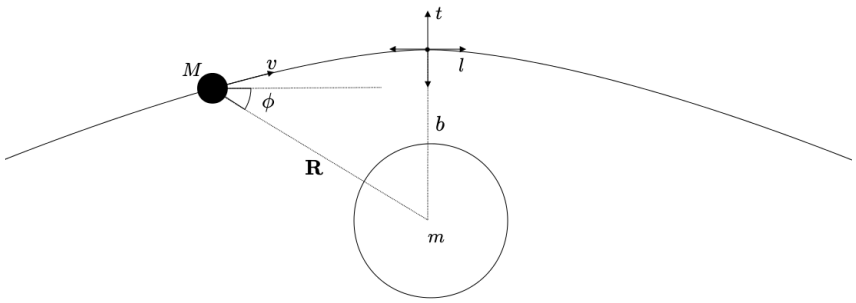

Figure 3: Collision diagram for a hyperbolic trajectory.

2.5 Displacement Amplitudes and Energy Transfer

We now define a 2D coordinate system consisting of two orthogonal directions denoted longitudinal l and transverse t such that the l-direction is parallel to the FSO's trajectory at time $t = 0$, and the t direction is perpendicular to it and runs through the center of the star, as shown in figure 3. We then split the force $\mathbf{f}$ in Eq. (16) into longitudinal and transverse components, denoted by f_l and f_t, respectively. The magnitude of these forces are $f_l = f\cos\phi$ and $f_t = f\sin\phi$, where $\phi(t)$ is the angle between the longitudinal direction and $\mathbf{R}$. In general, we will use the subscript n to refer to both the l and t components.

In order to deal with the multiple derivatives of x included in equation (16), we perform a Fourier transform on $x_n(t)$ and $f_n(t)$. The full derivation is described in detail in Appendix A. We Fourier transform $f(t)$ and $x(t)$ so that

$$\tilde{f}_n(\omega) = \frac{1}{\sqrt{2\pi}}\int_{-\infty}^{\infty} f_n(t)e^{i\omega t}dt, \tag{23}$$

which leads to the solution of Eq. (16) as

$$\tilde{f}_n(\omega) = [\omega_0^2 - \omega^2 - 2i\beta\omega]\tilde{x}_n(\omega), \tag{24}$$

or

$$\tilde{x}_n(\omega) = \frac{\tilde{f}_n(\omega)}{\omega_0^2 - \omega^2 - 2i\beta\omega}. \tag{25}$$

Its magnitude squared is

$$|\tilde{x}_n(\omega)|^2 = \frac{\tilde{f}_n(\omega)}{(\omega_0^2 - \omega^2 - 2i\beta\omega)}\frac{\tilde{f}_n^*(\omega)}{(\omega_0^2 - \omega^2 + 2i\beta\omega)} = \frac{|\tilde{f}_n(\omega)|^2}{(\omega_0^2 - \omega^2)^2 + 4\beta^2\omega^2}. \tag{26}$$

The values of ω carried by the time-dependent gravitational field close to ω_0 will have a much larger (resonating) effect on the star, while values of ω far from ω_0 have little significance.

The total energy transferred onto the star in the collision is given by

$$\Delta E = \sum_{n=l,t}\int_{-\infty}^{\infty} F_n(t)\dot{x}_n(t)dt. \tag{27}$$

In terms of the Fourier transform $\tilde{F}$ and $\tilde{x}$, (see Appendix B) we obtain

$$\Delta E = \frac{1}{\pi}\sum_{n=l,t}\int_0^{\infty} \omega\mathcal{R}e\left[i\tilde{F}_n(\omega)\tilde{x}_n^*(\omega)\right]d\omega. \tag{28}$$

Now we have all the information required to describe the collision and resulting oscillation, except for a model of the trajectory itself, which will give us values for $R(t)$ and $\phi(t)$ as required by equation (6) and

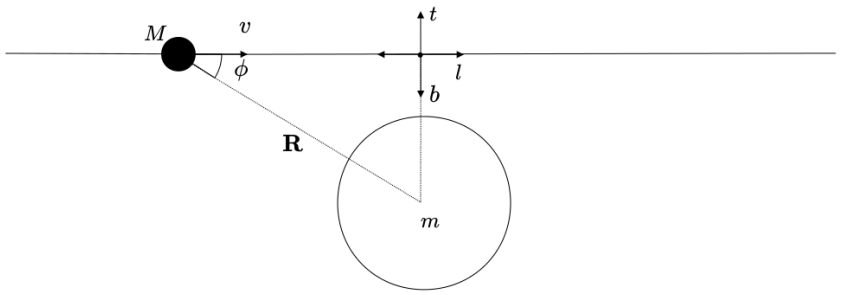

Figure 4: Collision diagram for a straight-line motion.

the definitions of the l and t components of F. In the following two sections, we will consider two different trajectory models: first a hyperbolic trajectory and second a straight-line approximation. The hyperbolic trajectory follows Kepler's laws and is the more accurate. But the equations for hyperbolic motion are parametrized such that only a numerical solution is possible. The straight-line approximation, on the other hand, is analytically soluble, and captures most of the physics of the problem.

2.6 Hyperbolic Trajectories

From Kepler's laws, three parameters define the hyperbolic orbit:

- e, Eccentricity of the orbit, $e > 1$ for hyperbolic orbit;
- α, Semi-major axis, α is negative for hyperbolic orbit;
- k, Gravitational parameter, $k = G(M + m)$.

We define an angle θ characterizing the angle along the orbital motion such that $\theta = 0$ is at the point of closest approach. There is no explicit equation to give R as a function of t, but by using θ as a parameter, we can formulate parametric equations that yield R and t as functions of θ, thereby giving a method to find discrete values of $R(t)$.

According to Kepler's Law, the distance R between the two objects is given by:

$$R(\theta) = \frac{\alpha(1 - e^2)}{1 + e\cos(\theta)}. \tag{29}$$

Since $\theta = 0$ at periapsis, the distance of closest approach is $a = \alpha(1 - e)$ [13]. For a collision with impact parameter b the relationship with these variables is obtained through $a = 2b/(\beta + \sqrt{\beta^2 + 4})$ where $\beta = GMm/(Eb)$, $E = \mu v^2/2$ is the collision energy and $\mu = Mm/(m + M)$ is the reduced mass.

The time dependence of the orbit is obtained from the equations

$$H = \cosh^{-1}\left(\frac{e + \cos(\theta)}{1 + e\cos(\theta)}\right) \tag{30}$$

and

$$t - t_0 = [(-\alpha)^3/k]^{1/2}\,(e\sinh(H) - H)\,, \tag{31}$$

where H is called the *hyperbolic anomaly*.

We can now use this trajectory, along with equations (6) and (25) to model the oscillations of a star induced by the passage of a massive object.

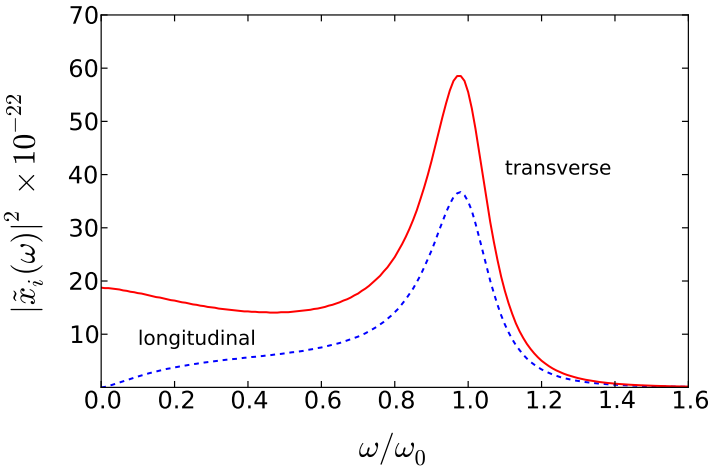

Figure 5: The amplitudes $|\tilde{x}|^2$ multiplied by 10^{22} (m^2 s^2 units) as a function of the oscillation frequency, for longitudinal (dashed blue line) and transverse (solid red line) oscillations. In this collision, $M = 2M_\odot$, $v = 1000$ km/s, $b = 5R_\odot$, $m_s = M_\odot$, $r_s = R_\odot$, and $A_\gamma = 0.1$.

2.7 Straight-Line Approximation

The straight line trajectory is a reasonable approximation when the eccentricity of the hyperbolic orbit is large.

In using the assumption of a straight line, the velocity is constant throughout the collision, so the distance away from the point of closest approach (where $t = 0$) is given by vt. Also, in this approximation the impact parameter b remains unchanged, and is simply defined as the distance of closest approach. As such, the distance R between the two objects has a simple formula using the Pythagorean theorem (see figure 4):

$$R(t) = \sqrt{b^2 + v^2t^2}. \tag{32}$$

Additionally, the sine and cosine of angle $\phi(t)$ are easily defined (see figure 4):

$$\cos\phi = \frac{vt}{\sqrt{b^2 + v^2t^2}} \; ; \; \sin\phi = \frac{b}{\sqrt{b^2 + v^2t^2}}. \tag{33}$$

Hence, we can easily separate the longitudinal and transverse components of the force using equation (10).

Specifically, fhe longitudinal portion of the force is given by

$$f_l(t) = f(t)\cos\phi = \frac{GMvt}{(b^2 + v^2t^2)^{3/2}}. \tag{34}$$

Performing a Fourier transformation, we have

$$\tilde{f}_l(\omega) = \frac{1}{\sqrt{2\pi}} \int_{-\infty}^{\infty} \frac{GMvt}{(b^2 + v^2t^2)^{3/2}} (\cos\omega t + i\sin\omega t) dt. \tag{35}$$

The integrand of this function has an even and an odd portion. The odd term drops out, and

$$\tilde{f}_l(\omega) = i\sqrt{\frac{2}{\pi}} \int_0^{\infty} \frac{GMvt\sin\omega t}{(b^2 + v^2t^2)^{3/2}} dt, \tag{36}$$

which can be solved analytically to give

$$\tilde{f}_l(\omega) = \sqrt{\frac{2}{\pi}} \frac{iGM\omega}{v^2} K_0\left(\frac{\omega b}{v}\right) = \sqrt{\frac{2}{\pi}} \frac{iGM}{bv} \xi K_0(\xi), \tag{37}$$

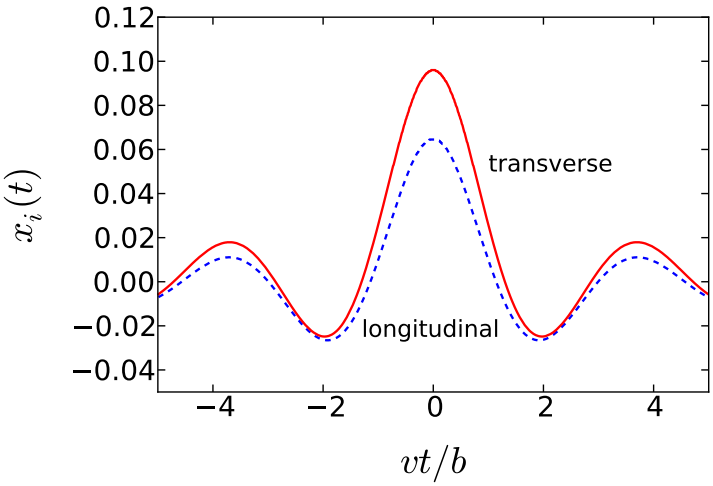

Figure 6: Oscillation amplitudes in units of the stellar radius as a function of time. The collision parameters are the same as in figure 5.

where K_0 is the modified Bessel function of the second kind with order zero, and $\xi = \omega b/v$.

For the transverse portion of the force,

$$f_t(t) = f(t)\sin\phi = \frac{GMb}{\left(b^2 + v^2t^2\right)^{3/2}}, \tag{38}$$

which undergoes a Fourier transform and similar odd/even elimination, resulting in

$$\tilde{f}_t(\omega) = \sqrt{\frac{2}{\pi}}\int_0^\infty \frac{GMb\cos\omega t}{\left(b^2 + v^2t^2\right)^{3/2}}dt. \tag{39}$$

This integral has the analytical solution

$$\tilde{f}_t(\omega) = \sqrt{\frac{2}{\pi}}\frac{GMb\omega}{v^2}K_1\left(\frac{\omega b}{v}\right) = \sqrt{\frac{2}{\pi}}\frac{GMm}{bv}\xi K_1(\xi), \tag{40}$$

where K_1 is the modified Bessel function of the second kind with order one.

3 Results

3.1 Main Sequence Star

To model the response of a typical main sequence star, we chose solar-type star with mass and radius values $m_s \sim M_\odot$ and $r_s \sim R_\odot$. As discussed in Section 1.4, let us make an estimate of the parameters for the resonant condition. For a collision with an impact parameter b, the "collision time", i.e. the time during which the gravitational force is most effective, is given $t_{coll} \sim b/v$. For a collision with $b = 5r_\odot$ and $v = 1000$ km/s, one gets $t_{coll} \sim 1$ h. The period of the oscillations associated with Eq. (17) for a solar-type star is given by $t_{osc} = 2\pi/\omega_0 \sim 3$ h. Hence, we expect a large resonating response for oscillations in this system for impact parameters in the range of a few times r_s.

Figure 5 shows the response of the star to oscillations at a specific wavelength ω. The amplitudes $|\tilde{x}|^2$ are multiplied by 10^{22} ($\mathrm{m}^2\ \mathrm{s}^2$ units) and shown for longitudinal (dashed blue line) and transverse (solid red line) oscillations. In this collision, $M = 2M_\odot$, $v = 1000$ km/s, $b = 5R_\odot$, $m_s = M_\odot$, $r_s = R_\odot$, and $A_\gamma = 0.1$. The peak at ω/ω_0 is not surprising, since any system will oscillate more significantly around its natural harmonic. One important thing which this graph shows is that oscillation cuts off sharply for values higher than $1.4\omega_0$.

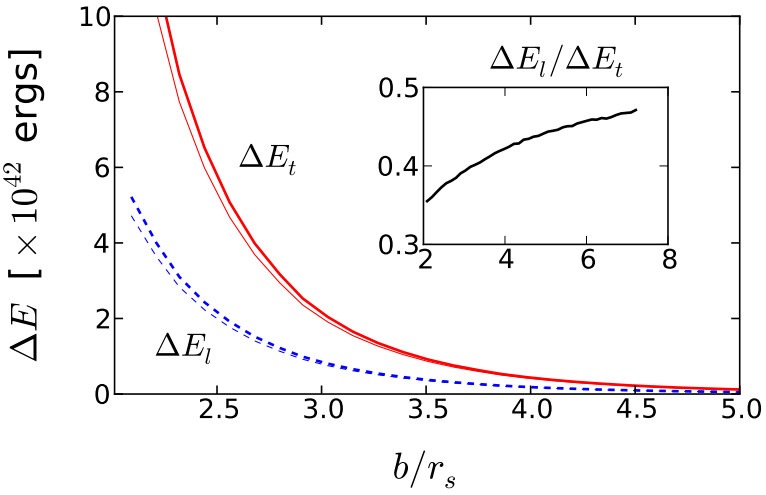

Figure 7: Energy, in ergs, transferred to stellar oscillations along longitudinal (l, dashed blue line) and perpendicular (t, solid red line) directions as a function of the impact parameter in units of the star radius. The thin (lower) lines represent calculations using parametrized hyperbolic trajectories, while the thick lines represent the straight-line approximation. The inset shows the ratio between the two energies. $M = 2M_\odot$, $v = 1000$ km/s, $m_s = M_\odot$, and $A_\gamma = 0.1$.

Also, we see from this graph that the transverse component of the oscillation is greater in magnitude than the longitudinal portion, a feature which we will see repeated in the following results.

Figure 6 shows the total tidal displacement as a function of time. According to these results, the star will be distorted from a spherical shape by approximately 10% at maximum distortion. This is in fact larger than any observed stellar oscillation, and would be very significant if observed. At time $t = 0$, the magnitude of these oscillations is too large for the small-amplitude assumption of our basic forced harmonic oscillator model, which indicates that we should use a accurate non-linear model. Also, we see from this figure the total length in time of the oscillations following the collision. As we can see from the graph, significant bulk oscillation continues for more than 10 multiples of the collision time. The resultant oscillation would be seen for some time after the actual collision takes place. This figure also shows that the longitudinal oscillations are smaller in magnitude than transverse oscillations, but this difference is small.

Figure 7 contains the most interesting results of this study. This graph indicates that for an impact parameter on the scale of $1 - 5R_\odot$, the amount of energy transferred to the stationary star is on the order of 10^{42} ergs. This value is approximately the same as the total energy radiated by the Sun in one year, and is also similar to the amount of energy released in an x-ray burst from an accreting neutron star in a binary system [14]. If the energy is all emitted quickly (in a few hours or days), the burst of radiation would be very significant, and possibly observable from Earth. The timescale of such emissions depends on the internal structure of the star, so we cannot make a prediction as to the actual emission of this energy using this model.

Figure 7 also shows the accuracy of the straight-line approximation (thin lines) as compared to the fully hyperbolic trajectory calculation (thick lines). It is clear from the graph that for smaller impact parameters the straight-line approach is less accurate, but the differences decreases for larger impact parameters. This difference makes sense because a collision with a small impact parameter would distort the trajectory more strongly.

The inset of figure 7 shows the impact parameter dependence of transverse and longitudinal components of the oscillation. Following the same trend, it is clear that the two yield an equal contribution as the impact parameter increases.

3.2 Compact Stars

Now we consider compact stars (WD and NS, discussed in Sections 1.3.2 & 1.3.3) in addition to main sequence stars. For reference, we choose a stellar mass $m_s = 1.4M_\odot$, since it is physically possible for all three stellar types. We choose r_s for each type of star according to accepted mass/radius relations.

First, we consider the response of each type of star to a collision at $b = 5R_\odot$, the same impact parameter used for the previous study of solar-type stars. The energy transfer and maximum effective displacement for each of these collisions is given in Table 1. From these results, it is clear that induced stellar oscillations not only have a far lesser magnitude in compact stars, but also impart far less energy than in collisions with solar-type stars. Such a result makes sense because the higher density of compact stars results in a much higher natural oscillation frequency, so we do not achieve the resonant condition as in the collisions with solar-type stars.

r_s(km)	ΔE_l(ergs)	ΔE_t(ergs)	x_{max}/r_s
7 x 10^5 (solar-type)	0.324 x 10^{42}	0.608 x 10^{42}	0.128
7 x 10^3 (WD)	1.76 x 10^{32}	1.88 x 10^{32}	1.07 x 10^{-5}
10 (NS)	1.09 x 10^2	2.09 x 10^2	0.986 x 10^{-22}

Table 1: Induced oscillation for different types of star at impact parameter $b = 5R_\odot$. $M = 2M_\odot$, $v = 1000$ km/s, $b = 5R_\odot$, $m_s = 1.4M_\odot$, and $A_\gamma = 0.1$.

Next we consider collisions of compact stars with a smaller impact parameter. In particular, we are interested in $b = 5r_s$, where r_s is the radius of the compact star involved in the collision. For these interactions, the colliding object must be a compact star or a black hole, since these impact parameters are actually smaller than the radius of a solar-type star. A collision with a solar-type star at such close distances would result in the smaller star passing inside the radius of the larger star, which cannot be accurately described by our model. Also, in the case of such close collisions, the passing object's trajectory is significantly altered by the compact star's gravitational field, so the straight-line approximation is no longer valid and we must use the hyperbolic trajectory (described in Section 2.6) to model the collision. The gravitational fields are so great in the NS collision that relativistic effects are likely to be significant. Our model does not consider relativity, however, so the results for the NS collision at $b = 5R_{NS}$ are probably not as accurate.

r_s(km)	b	ΔE_l(ergs)	ΔE_t(ergs)	x_{max}/r_s
7 x 10^3 (WD)	$5R_{WD}$	1.75 x 10^{43}	3.28 x 10^{43}	0.101
10 (NS)	$5R_{WD}$	4.56 x 10^{27}	1.92 x 10^{28}	4.17 x 10^{-6}
10 (NS)	$5R_{NS}$	1.19 x 10^{46}	2.27 x 10^{46}	0.102

Table 2: Induced oscillation for different types of star at smaller impact parameters. $M = 2M_\odot$, $v = 1000$ km/s, $b = 5R_\odot$, $m_s = 1.4M_\odot$, and $A_\gamma = 0.1$.

As we see in Table 2, the response for compact stars at smaller impact parameters is much more significant. In fact, the energy transfer for collisions at 5 times the stellar radius for compact stars is slightly higher than that of solar-type stars (rows 2 & 4 of the Table 2, and row 2 of 1). The proportional change in radius (5th column) also resembles that of a solar-type star, which is a significant finding especially for compact stars, as their high gravity makes them very close to perfect spheres at equilibrium. Although the induced oscillations for collisions of compact stars with small impact parameters are similar in magnitude to those modeled for solar-type stars, collisions within such a small impact parameter would be far less common than collisions with the previous conditions. However, the tidal excitation of a NS in particular is hypothesized to result in sudden emissions of radiation (gamma-ray or x-ray bursts, which can be observed from Earth) [15]. Hence, close collisions like this could have very profound effects on compact stars, despite their relative rarity.

4 Neutron Star Equation of State

In considering the density profile of neutron stars (NS), we have included an in-depth examination of the equation of state (EOS). This section is a summary of the results of previous research that was presented at a meeting of the Texas Section of the American Physical Society at Texas Tech University in Fall 2012 and at Tarleton State University in Spring 2013.

4.1 Introduction

Continuing with the discussion from Section 1.3.3, we will give a more in-depth overview of NS. The matter inside a neutron star is so densely packed that it becomes energetically favorable for most of the electrons to be captured by protons, forming an extremely high proportion of neutrons (hence the name neutron star). The following is a layer-by-layer description of the internal structure of a NS, noting the state of the protons and neutrons (collectively nucleons) which make up the star.

The outermost layer of the NS is the outer crust, where densely packed iron and lighter nuclei dominate. In this region, there is still significant spacing between nuclei, although it still a fraction of the distance between nuclei in terrestrial matter.

Deeper into the crust, nuclei become heavier and more neutron-rich, as well as more densely packed. Eventually, the nuclei become so full of neutrons that they begin to become unbound from their respective nuclei. This point is referred to as the neutron drip line. Further in, free neutrons become more common and nuclei become smaller and rarer under the pressure of gravity. Also, in this region there is the possibility of interesting states of matter called pasta phases, in which first free neutrons and then nuclei become stretched by gravity to form uniquely shaped matrices of superdense matter.

The core is defined to begin where individual nuclei disappear entirely. This leaves a "sea of neutrons" called a neutron Fermi liquid, with few protons scattered throughout. The dominance of free nucleons in this region leads to the term nuclear matter to describe the matter inside a neutron star. The great majority of the star's mass is found within the core and inner core, which makes the internal structure vital to any accurate description of NS.

Last is the inner core, where nuclei themselves are expected to collapse under gravity. There is much speculation about the exact nature of matter in the inner core, but it is certain to be some extremely exotic form of matter: possibly a quark-gluon plasma, "strange" matter made up of heavier-than-nucleon baryons, or some other unfamiliar form of matter. This is another of the interesting applications of NS research, as finding an accurate model for NS bulk structure would yield some data about the matter in this otherwise inexplorable region.

4.2 Structure Equations

In determining the structure of a neutron star, we consider the following differential equations:

1. Equation of Mass Conservation:
$$\frac{dM(r)}{dr} = 4\pi r^2 \rho(r) \tag{41}$$

2. Tolmann-Oppenheimer-Volkoff (TOV) Equation:
$$\frac{dP(r)}{dr} = -\frac{G}{r^2}\left[\rho(r) + \frac{P(r)}{c^2}\right]\left[M(r) + 4\pi r^3 \frac{P(r)}{c^2}\right]\left[1 - \frac{2GM(r)}{c^2 r}\right]^{-1} \tag{42}$$

(where $M(r)$ is the total mass inside radius r, ρ is density, P is pressure, G is the gravitational constant, and c is the speed of light).

In order to solve these two equations, we must also formulate an equation of state (EOS), which gives the pressure as a function of density, $P(\rho)$. Once an EOS is chosen, these equations can be solved numerically using a modified Runge-Kutta method, where we choose a central density ρ_c and begin from the center, integrating outwards over the entire star.

In our previous work with the collision and oscillation of NS, we simplified the problem by assuming incompressibility and homogeneity of stellar matter. As such, we do not directly apply the above equations,

nor any of the EOS explored here, to the stellar oscillation model. However, the mass and radius values used in modeling NS oscillation were derived from the mass and radius values presented in the results of this section, which were determined using the above equations and an accurate EOS. In the future, we plan to include the results in this section to the stellar collision model described previously.

4.3 "Correct" EOS

As of the time of writing, the "correct" EOS is not known. Since nuclear matter is too exotic to duplicate on Earth, the exact properties of this matter can only be estimated according to the known laws of physics. Using these estimations, many possible candidates for accurate EOS have emerged. Each of these EOS predict different large-scale properties (total mass and radius) for NS when solved in conjunction with Eqs. (41) & (42), so observations should help to limit the range of accurate EOS.

Unfortunately, NS are difficult to observe from Earth, and their large-scale properties are only now beginning to be observed using indirect astronomical methods with a high degree of observational and systematic error. However limited, we can still use these observations to narrow down the search for an accurate EOS. We have modeled several modern candidates for neutron star equations of state and compared the resulting values to the limited astronomical observations.

4.4 Two Types of Model

There are two predominant classes of model for calculating the EOS for dense nuclear matter. Both can be used to find semi-accurate models for NS and are accurate within known parameters according to quantum mechanics and properties of terrestrial nuclei.

4.4.1 "Effective" Models

Since NS are mostly made up of densely packed nucleons (protons and neutrons, which make up nuclei in normal matter) and average a density near that of an atomic nucleus, a NS can be considered like a very large nucleus. As such, we can look to the properties of large nuclei on Earth as a basic guide for the structure of NS. Effective models begin by determining how nuclei interact within a large atomic nucleus, and then infer bulk properties of nuclear matter. This data can then be applied to the whole NS.

4.4.2 "Realistic" Models

Realistic models avoid the large-nucleus approximations, and instead attempt to describe the properties of dense matter beginning with the fundamentals of quantum mechanics. That is, nuclear matter in a neutron star is simply a large number of closely packed nucleons. The interactions between two nucleons are well known, as described by quantum mechanics. Following the same rules, the interactions between three nucleons can be described. Continuing outward, the properties of a large cluster of nuclear matter can be extrapolated, and then a whole NS.

4.5 Equations Modeled

The equations considered in this study are listed below:

- APR [16]
- Glendenning [17]
- SKMS [18]
- SLY4 [19]
- FSUGold [20]
- NL3 [21]
- WFF [22]

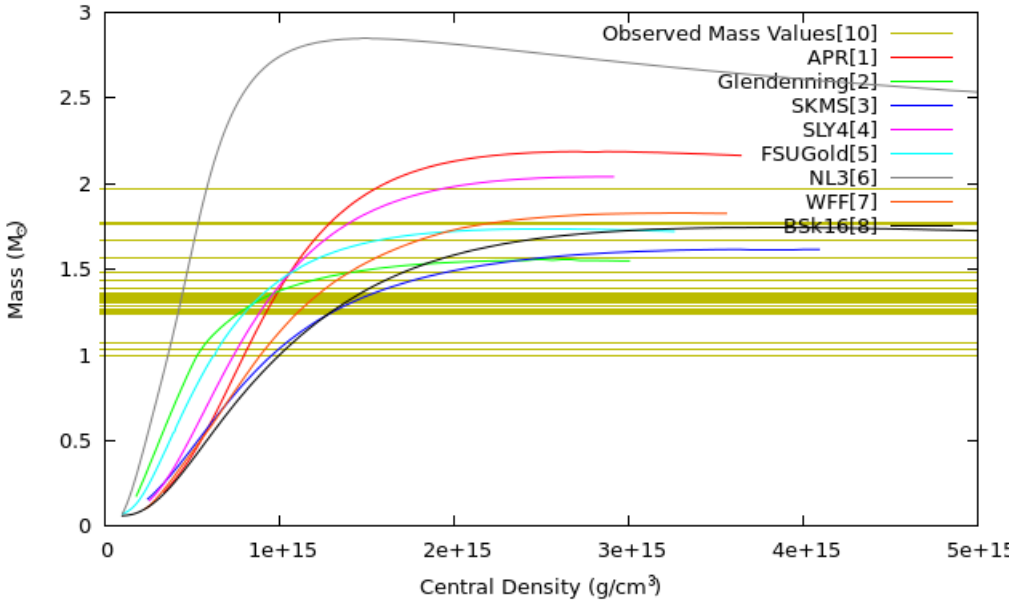

Figure 8: Mass as a function of central density

- BSk16 [23]

4.6 Observations

In order to compare the accuracy of proposed EOS, we need some observations of actual NS. The observations used in this comparison are from two different studies which use different methods to find bulk NS properties. Both have results which lie within the generally accepted probable range for NS.

4.6.1 Mass

The observed masses we use are from Ref. [25]. The observations themselves are from NS that is a part of a binary system, with the other being a directly observable luminous star. Since the mass values are calculated based on Kepler's Laws, the chief inaccuracy is observational, and so values are correct to a much higher accuracy than the radius observations discussed in the next section. These mass values are compared with predicted mass values as a function of the star's density in figure 8.

4.6.2 Mass and Radius

The mass and radius observations come from a certain type of binary system called x-ray burst binaries. These binaries are composed of a neutron star and a less dense companion star, such as a main sequence star or a white dwarf. In these systems, some of the matter of the companion star is slowly pulled away from its original star and towards the NS due to its strong gravity, a process called accretion. As this matter reaches the NS surface, it is subject to a very strong gravity which results in the accreted matter's gravitational energy being released suddenly in the form of x-rays. These sudden bursts of radiation can be measured on Earth, and can lead to conclusions about the originating mass. In Ref. [24] one infers the radius of the NS based on the properties of these x-ray emissions, and the mass based on Kepler's Laws (as above). However, this method is not well-accepted and so the systematic error is higher than usual (which is indicated in figure 9 by the large error boxes).

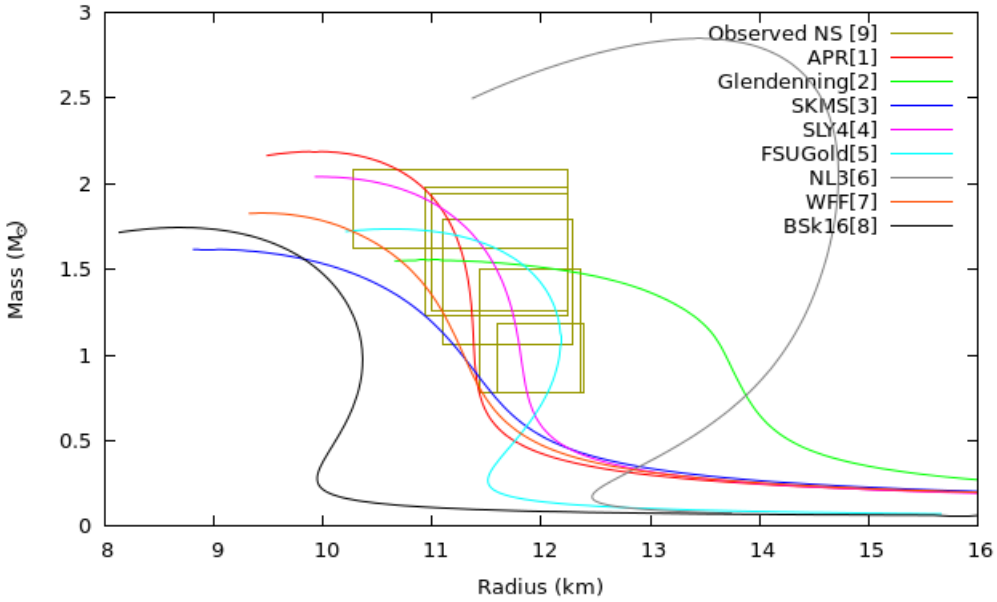

Figure 9: Mass as a function of radius

4.7 Results

Colored curves on figure 8 show the masses as predicted by a particular EOS. The yellow horizontal lines show the observed NS masses. This diagram demonstrates a feature of the TOV equation called the TOV limit. Following the colored lines, it is clear to see that each EOS predicts a maximum possible mass, and masses either plateau or fall slightly after this peak. This maximum mass is called the TOV limit (the Chandresekhar limit in white dwarfs is a similar and better-known phenomenon), and is a feature of the TOV equation, rather than the individual EOS. The TOV limit is the maximum possible mass for a NS, and at any greater mass, nucleons will break down and the star will collapse, forming either a quark star (whose existence is hypothesized but not confirmed) or it will collapse entirely into a black hole. As figure 8 illustrates, each EOS predicts a slightly different TOV limit. Since no NS can exist with a mass higher than the TOV limit, any proposed EOS which has a TOV limit lower than any of the observed masses is therefore inaccurate and can be eliminated from the search for an accurate EOS. As illustrated in this graph, many of the proposed EOS curves fall short of highest observed mass. So now we focus only on the proposed EOS which satisfy this constraint on mass, which are the APR, SLY4, and NL3 equations of state.

In order to narrow the search further, we consider the observed masses and radii of NS. Unfortunately, the method of finding these two quantities together has a high uncertainty and the error bounds are wide for each observation. As such, we will say that any EOS which roughly follows this trend is supported by mass and radius observations. Figure 9 displays the mass-radius curves of different EOS as colored curves, and the approximate range for observed masses and radii as yellow rectangles. Looking at the three EOS which satisfy the previous paragraph's restrictions on mass, we see that while the mass-radius curves for the APR and SLY4 EOS approximately fall under the same region as the observations, the NL3 curve is clearly outside of the accurate region. As such, we conclude that from the selection tested here, only the APR and SLY4 EOS remain possible candidates in the search for an accurate equation of state.

5 Appendices

5.1 Appendix A - Fourier Transform

Beginning with equation (16), we perform a Fourier transform. Let

$$f(t) = \frac{1}{\sqrt{2\pi}} \int_{-\infty}^{\infty} \tilde{f}(\omega) e^{-i\omega t} d\omega. \tag{43}$$

So then

$$\tilde{f}(\omega) = \frac{1}{\sqrt{2\pi}} \int_{-\infty}^{\infty} f(t') e^{i\omega t'} dt' \tag{44}$$

We can prove that (43) implies (44) by substituting the second into the first, as follows

$$f(t) = \frac{1}{\sqrt{2\pi}} \int_{-\infty}^{\infty} \left[\frac{1}{\sqrt{2\pi}} \int_{-\infty}^{\infty} f(t') e^{i\omega t'} dt' \right] e^{-i\omega t} d\omega \tag{45}$$

which can be rearranged to form

$$f(t) = \int_{-\infty}^{\infty} f(t') \left[\frac{1}{2\pi} \int_{-\infty}^{\infty} e^{i\omega(t'-t)} d\omega \right] dt'. \tag{46}$$

The inner integral in this equation is the delta function for $t' - t$ by the Fourier Integral Theorem, so

$$f(t) = \int_{-\infty}^{\infty} f(t') \left[\delta(t' - t) \right] dt' = \begin{cases} 0 & \text{if } t' \neq t \\ f(t') & \text{if } t' = t \end{cases} = f(t). \tag{47}$$

Similarly, $x(t)$ can be expressed as a function of t and ω as well, with $\tilde{x}(\omega)$ defined analogous to $\tilde{f}(\omega)$

$$x(t) = \frac{1}{\sqrt{2\pi}} \int_{-\infty}^{\infty} \tilde{x}(\omega) e^{-i\omega t} d\omega. \tag{48}$$

Using this form allows derivatives to be taken easily, yielding the first derivative

$$\dot{x}(t) = \frac{d}{dt} \left[\frac{1}{\sqrt{2\pi}} \int_{-\infty}^{\infty} \tilde{x}(\omega) e^{-i\omega t} d\omega \right] = \frac{-i}{\sqrt{2\pi}} \int_{-\infty}^{\infty} \omega \tilde{x}(\omega) e^{-i\omega t} d\omega \tag{49}$$

and the second derivate

$$\ddot{x}(t) = \frac{d^2}{dt^2} \left[\frac{1}{\sqrt{2\pi}} \int_{-\infty}^{\infty} \tilde{x}(\omega) e^{-i\omega t} d\omega \right] = \frac{-1}{\sqrt{2\pi}} \int_{-\infty}^{\infty} \omega^2 \tilde{x}(\omega) e^{-i\omega t} d\omega. \tag{50}$$

Incorporating this new form for the $f(t)$, $x(t)$, and their derivatives, (16) can be rewritten as

$$\begin{aligned} 0 = \frac{-1}{\sqrt{2\pi}} \int_{-\infty}^{\infty} \omega^2 \tilde{x}(\omega) e^{-i\omega t} d\omega + 2\beta \frac{-i}{\sqrt{2\pi}} \int_{-\infty}^{\infty} \omega \tilde{x}(\omega) e^{-i\omega t} d\omega \\ + \omega_0^2 \frac{1}{\sqrt{2\pi}} \int_{-\infty}^{\infty} \tilde{x}(\omega) e^{-i\omega t} d\omega - \frac{1}{\sqrt{2\pi}} \int_{-\infty}^{\infty} \tilde{f}(\omega) e^{-i\omega t} d\omega. \end{aligned} \tag{51}$$

After combining terms, this is

$$0 = \frac{1}{\sqrt{2\pi}} \int_{-\infty}^{\infty} \left[-\omega^2 \tilde{x}(\omega) - 2i\beta\omega \tilde{x}(\omega) + \omega_0^2 \tilde{x}(\omega) - \tilde{f}(\omega) \right] e^{-i\omega t} d\omega. \tag{52}$$

Since this is valid for every value of t, the integrand must be zero,

$$-\omega^2 \tilde{x}(\omega) - 2i\beta\omega \tilde{x}(\omega) + \omega_0^2 \tilde{x}(\omega) - \tilde{f}(\omega) = 0 \tag{53}$$

which is solved for $\tilde{x}(\omega)$ algebraically,

$$\tilde{x}(\omega) = \frac{\tilde{f}(\omega)}{(\omega_0^2 - \omega^2 - 2i\beta\omega)}. \tag{54}$$

This result is the same as equation (25).

5.2 Appendix B - Derivation of ΔE

Beginning with the energy equation (27) and using a Fourier transform on the two functions F and $\dot{x}$, we have

$$F_n(t) = \frac{1}{\sqrt{2\pi}} \int_{-\infty}^{\infty} \tilde{F}_n(\omega) e^{-i\omega t} d\omega \tag{55}$$

$$\dot{x}_n(t) = \frac{\partial}{\partial t} x_n(t) = \frac{\partial}{\partial t} \left[\frac{1}{\sqrt{2\pi}} \int_{-\infty}^{\infty} \tilde{x}_n(\omega) e^{-i\omega t} d\omega \right] = \frac{1}{\sqrt{2\pi}} \int_{-\infty}^{\infty} -i\omega \tilde{x}_n(\omega) e^{-i\omega t} d\omega. \tag{56}$$

Taking the product of these two functions, we perform a double integral

$$\int F_n(t) \dot{x}_n(t) dt = \int \left[\frac{-i}{2\pi} \int \int \omega \tilde{x}_n(\omega) \tilde{F}(\omega') e^{-i(\omega+\omega')t} d\omega d\omega' \right] dt. \tag{57}$$

The integral over t yields the delta function $\delta(\omega - \omega')$. The resulting integral is

$$\Delta E = \frac{-i}{2\pi} \int \int \tilde{F}(\omega) \omega' \tilde{x}_n(\omega') \delta(\omega - \omega') d\omega d\omega' = \frac{-i}{2\pi} \int_{-\infty}^{\infty} (-\omega) \tilde{F}_n(\omega) \tilde{x}_n(-\omega) d\omega. \tag{58}$$

Since ω is real and $\tilde{x}$ is a Fourier function defined by

$$\tilde{x}(\omega) \equiv \int e^{-i\omega t} x(t) dt, \tag{59}$$

we see that $\tilde{x}(-\omega) = \tilde{x}^*(\omega)$, where * represents the complex conjugate:

$$\tilde{x}(-\omega) = \int e^{i\omega t} x(t) dt = \int \big\{ \cos(-\omega t) + i \sin(-\omega t) \big\} x(t) = \int \big\{ \cos \omega t - i \sin \omega t \big\} x(t) = \tilde{x}^*(\omega). \tag{60}$$

This result is true for all Fourier-type functions of real variables, so we can also extend this property to the function $\tilde{F}(\omega)$. Applying this property to the energy equation, we get

$$\Delta E = \frac{i}{2\pi} \int_{-\infty}^{\infty} \omega \tilde{F}_n(\omega) \tilde{x}_n^*(\omega) d\omega. \tag{61}$$

This integral can be further split into two parts,

$$\Delta E = \frac{i}{2\pi} \left[\int_{-\infty}^{0} \omega \tilde{F}_n(\omega) \tilde{x}_n^*(\omega) d\omega + \int_{0}^{\infty} \omega \tilde{F}_n(\omega) \tilde{x}_n^*(\omega) d\omega \right]. \tag{62}$$

We simplify the first part using the substitution $\omega = -\omega'$, and $d\omega = -d\omega'$. This results in

$$\int_{\infty}^{0} (-\omega') \tilde{F}_n(-\omega') \tilde{x}_n^*(-\omega') (-d\omega') = - \int_{0}^{\infty} (\omega') \tilde{F}_n^*(\omega') \tilde{x}_n(\omega') d\omega', \tag{63}$$

using the conjugate property of Fourier functions as in (60). Combining this with the other part of the equation, we have

$$\Delta E = \frac{i}{2\pi} \int_{0}^{\infty} \omega \left[\tilde{F}_n(\omega) \tilde{x}_n^*(\omega) - \tilde{F}_n^*(\omega) \tilde{x}_n(\omega) \right] d\omega = \frac{1}{\pi} \int_{0}^{\infty} \omega \mathcal{R}e \left[i \tilde{F}_n(\omega) \tilde{x}_n^*(\omega) \right] d\omega, \tag{64}$$

which is the same as (28).

References

[1] W.H. Press and S.A. Teukolsky, Ap. J. 213, 183 (1977).

[2] "The Fundamentals of Stellar Astrophysics", George W. Collins, II, NASA Astrophysics Data System (ADS) (2003).

[3] "Stellar Oscillations", Jorgen Christensen-Dalsgaard, Aarhus Universitet (2014).

[4] J.M. Lattimer and D.N. Schramm, Ap. J. 192, L145 (1974).

[5] S. L. Shapiro and S. A. Teukolsky, "Black Holes, White Dwarfs and Neutron Stars" (Wiley, 1983).

[6] D. Tsang, Astrop. J. 777, 103 (2013).

[7] A. G. Kosovichev, American Institute of Physics Conference Series, Vol. 1170, 547559 (2009).

[8] W. R. Brown, M. J. Geller, S. J. Kenyon, and M. J. Kurtz, Astrophys. J. 622, L33 (2005).

[9] Hale Bradt, Astrophysics Processes, Cambridge University Press (2008), Chapter 4.

[10] Sir Thomson W (Lord Kelvin) 1863 Phil. Trans. (papers iii, 384).

[11] J. R. Nix, Ann. Phys. (N. Y.) 41, 52 (1967).

[12] Z. Kopal, Astrophysica Norvegica, 25, 239 (1964).

[13] "An Introduction to Celestial Mechanics", F. R. Moulton, Dover Publications (1984).

[14] G. Vedrenne and J.-L. Atteia, "Gamma-Ray Bursts: The brightest explosions in the Universe". Springer/Praxis Books. ISBN 978-3-540-39085-5. (2009).

[15] D. Tsang, J. S. Read, T. Hinderer, A. L. Piro, and R. Bondarescu, Phys. Rev. Lett. 109, 071102 (2012).

[16] A. Akmal, V. R. Pandharipande, and D. G. Ravenhall, Phys. Rev. C 58, 1804 (1998).

[17] N. Glendenning, Compact Stars, Springer-Verlag, 1997, pg.244.

[18] J. Bartel, P. Quentin, M. Brack, Nucl. Phys. A 386, 79 (1982).

[19] E. Chabanat, P. Bonche, P. Haensel, Nucl. Phys. A 627, 710 (1997).

[20] B. G. Todd-Rutel and J. Piekarewicz, Phys. Rev. Lett 95, 122501 (2005).

[21] G. A. Lalazissis, J. Konig, and P. Ring, Phys. Rev. C55, 540 (1997).

[22] R. B. Wiringa, V. Fiks, and A. Fabrocini, Phys. Rev. C 38, 1010 (1988).

[23] S.Goriely, N. Chamel, J.M. Pearson, Pys. Rev. Lett 102, 152503 (2010).

[24] A. W. Steiner, J. M. Lattimer and E. F. Brown, Astrophys. J. 722, 33 (2010).

[25] F. Ozel, D. Psaltis, R. Narayan, A. Santos Villarreal, Ap. J. 757, 55 (2012).